PCCP

Dynamic Article Links

Cite this: *Phys. Chem. Chem. Phys.*, 2011, **13**, 8653–8658

www.rsc.org/pccp

PAPER

Waveform control of orientation-dependent ionization of DCl in few-cycle laser fields

I. Znakovskaya,[a] P. von den Hoff,[b] N. Schirmel,[c] G. Urbasch,[c] S. Zherebtsov,[a] B. Bergues,[a] R. de Vivie-Riedle,*[b] K.-M. Weitzel*[c] and M. F. Kling*[ad]

Received 1st December 2010, Accepted 17th March 2011
DOI: 10.1039/c0cp02743j

Strong few-cycle light fields with stable electric field waveforms allow controlling electrons on time scales down to the attosecond domain. We have studied the dissociative ionization of randomly oriented DCl in 5 fs light fields at 720 nm in the tunneling regime. Momentum distributions of D^+ and Cl^+ fragments were recorded *via* velocity-map imaging. A waveform-dependent anti-correlated directional emission of D^+ and Cl^+ fragments is observed. Comparison of our results with calculations indicates that tailoring of the light field *via* the carrier envelope phase permits the control over the orientation of DCl^+ and in turn the directional emission of charged fragments upon the breakup of the molecular ion.

1. Introduction

Laser pulses with stable electric field waveforms of a few cycles duration allow us to control electronic motion on timescales reaching down to the attosecond regime.[1] Ultimately this is expected to provide means for controlling chemical processes.[2] The generation of laser pulses with a well-defined electric field waveform $E(t) = E_0(t)\cos(\omega t + \varphi)$, with envelope $E_0(t)$ and frequency ω, became possible by the stabilization of the carrier envelope phase (CEP) φ. CEP-stable few-cycle pulses have been applied to the control of electron localization in the dissociative ionization of the prototype molecules D_2,[3,4] HD[4] and H_2.[5] After initial ionization, these systems only contain a single electron. The steering of this electron is achieved *via* light-induced coherent superposition of two electronic states with CEP dependent amplitudes and phases. This process has been the subject of a large number of theoretical investigations (see *e.g.* ref. 6–10 and references cited therein). The light-field induced electron localization leads to a directional emission of charged and uncharged fragments upon the break-up of the molecule. The single-color CEP control is related to multi-color relative phase-control first introduced by Brumer and Shapiro.[11,12] Among many other studies, the $\omega_2 = 3\omega_1$ phase control of the ionization and dissociation of a variety of diatomic molecules has been investigated (see *e.g.* ref. 13 and 14). As a recent example in the femtosecond domain, studies using a two-color laser field $E(t) = E_1(t)\cos(\omega t) + E_2(t)\cos(2\omega t + \varphi_{\text{two-color}})$ with ω and 2ω corresponding to 800 nm and 400 nm, respectively, have shown that the directional emission of D^+ and D fragments from the dissociative ionization of D_2 can be tailored with the relative phase $\varphi_{\text{two-color}}$.[15]

Light-waveform control of electron dynamics in a more complex molecule was recently demonstrated for carbon monoxide.[16,17] In this study, 4 fs, linearly polarized laser pulses at 740 nm and an intensity of 8×10^{13} W cm^{-2} have been applied to dissociatively ionize CO. Quantum calculations indicated that two mechanisms are responsible for the observed asymmetry in the C^+ and O^+ ion emission. First, the ionization of CO in a near-single cycle phase-stable laser field is found to be orientation-dependent.[18] Second, excitation of CO^+ by the laser-driven recolliding electron, that was freed in the first ionization step, leads to dissociation and laser-induced coupling of potential energy curves of CO^+, resulting in the formation of $C^+ + O$ and $C + O^+$ and a CEP dependent asymmetry.[17] In this particular study, the individual contributions from the two mechanisms could not be clearly distinguished from the experimental data.

Here, we report on studies on the dissociative ionization of DCl in few-cycle CEP-stable laser fields. DCl is an interesting target, for which the fragmentation channels $Cl^+ + D$ and $Cl + D^+$ are well known (see *e.g.* ref. 19 and 20). While the CEP dependent fragmentation of DCl^+ has been investigated theoretically,[21] no experimental study on the CEP control of the dissociative ionization of DCl in few-cycle light fields was reported. In our experiments, velocity-map imaging was utilized to record the momentum distributions of D^+ and Cl^+ fragments from the dissociative ionization of DCl. We find an

[a] *Max-Planck-Institut für Quantenoptik, Hans-Kopfermann-Str. 1, 85748 Garching, Germany. E-mail: matthias.kling@mpq.mpg.de*
[b] *Department für Chemie und Biochemie, Ludwig-Maximilians-Universität München, 81377 München, Germany. E-mail: regina.de_vivie@cup.uni-muenchen.de*
[c] *Fachbereich Chemie, Philipps-Universität Marburg, Hans Meerweinstr., 35032 Marburg, Germany. E-mail: weitzel@chemie.uni-marburg.de*
[d] *J. R. Macdonald Laboratory, Department of Physics, Kansas State University, Manhattan, KS 66506, USA*

anti-correlated, CEP dependent directional emission of D^+ and Cl^+ fragments (the asymmetries of the D^+ and Cl^+ fragments are phase shifted by π). Our calculations indicate that the observed control at the chosen laser parameters can be explained by a single mechanism: the orientation-dependent ionization of DCl molecules that is controlled *via* the CEP of the few-cycle laser pulse.

2. Experimental results

The experimental scheme is similar to the one described in ref. 3. In brief, transform-limited, phase-stable laser pulses at 790 nm central wavelength of *ca.* 25 fs duration with 1 mJ energy per pulse at 1 kHz repetition rate have been generated by an amplified Ti:sapphire laser system (Femtopower Compact Pro, Femtolasers) at the AS-5 infrastructure at the Max Planck Institute of Quantum Optics. The pulses were spectrally broadened using a 1 m long hollow-core fiber of 250 μm diameter filled with 2.5 bar Neon gas. The laser pointing into the fiber was controlled with high precision using a commercial beam stabilization system (Beamlock, TEM Messtechnik). The output pulses from the fiber were compressed to a near-transform limited duration of $\sim$5 fs at a central wavelength of 720 nm in a chirped-mirror compressor. The pulse duration was monitored online with a commercial dispersion balanced autocorrelator (Femtometer, Femtolasers). The laser phase has been actively stabilized using two feedback loops as described in ref. 22. The phase jitter was smaller than 150 mrad. The CEP φ was varied in the experiment by insertion of dispersive material *via* a pair of wedged fused silica plates. The measured phase φ_{CEP} discussed in this paper contains a phase-offset φ_0 relative to the absolute phase φ: $\varphi_{CEP} = \varphi_0 + \varphi$. The phase offset φ_0 can be determined by comparing experimental data to theoretical predictions (see *e.g.* ref. 23).

The phase-stabilized, linearly polarized pulses were focused with a spherical mirror (f = 50 cm) into a velocity-map imaging (VMI) spectrometer.[24,25] A peak intensity in the focus of $1.3(\pm0.3) \times 10^{14}$ W cm^{-2} was determined from the cutoff in electron spectra recorded for Xe[23,26] under the same experimental conditions as for the molecular experiments. Ions or electrons that were generated at the laser focus in the VMI spectrometer were projected onto an MCP/phosphor screen assembly using a static electric field. The velocity map images have been recorded with a low-noise CCD camera (Sensicam, PCO). Different ionic species were distinguished by their time-of-flight (TOF) towards the detector and appropriate gating of the MCP with a laser-triggered, fast high-voltage switch (Behlke). 3D momentum distributions of recorded ions and electrons are obtained from the 2D projections by an iterative inversion procedure.[27] In the convention used here, the images lie in the x–y plane. The y-axis is the laser polarization axis and the axis of symmetry for the cylindrically symmetric VMI images. The polar angle θ is defined as the angle between a momentum vector $\vec{p}$ and the positive part of the y-axis, and the z-axis is the projection coordinate, lying along the detector (TOF) axis. Fig. 1 shows cuts through the 3D momentum distributions at p_z = 0 for D^+ and Cl^+ ions recorded without CEP stabilization. The laser is linearly polarized along the p_y-axis and propagates along p_x. Note that the signal from DCl^+ ions could not be completely suppressed in the recording of Cl^+ ions due to their close TOF proximity and the much stronger DCl^+ signal. The DCl^+ background in the center was therefore subtracted from the Cl^+ images, potentially obscuring Cl^+ signals at momenta below 20 a.u.

Within the axial recoil approximation and neglecting field-induced orientation, which is reasonable for the short pulses used here, the angle θ for the detected fragments reflects the orientation of the molecule. Both ionic species exhibit maxima in their angular distributions at angles around 60° relative to the laser polarization axis. For the D^+ ions concentric rings are visible at higher momenta, which are not visible in the Cl^+ data (note that the momentum resolutions were limited to 0.2 a.u. (D^+) and 0.4 a.u. (Cl^+)). Angular integrated energy spectra obtained from the images shown in Fig. 1 are shown in Fig. 2a and c for D^+ and Cl^+ ions, respectively.

In order to elucidate the effect of the CEP on the experimental ion momentum distributions, the phase φ_{CEP} was scanned over a range of 5π. In our analysis of the experimental

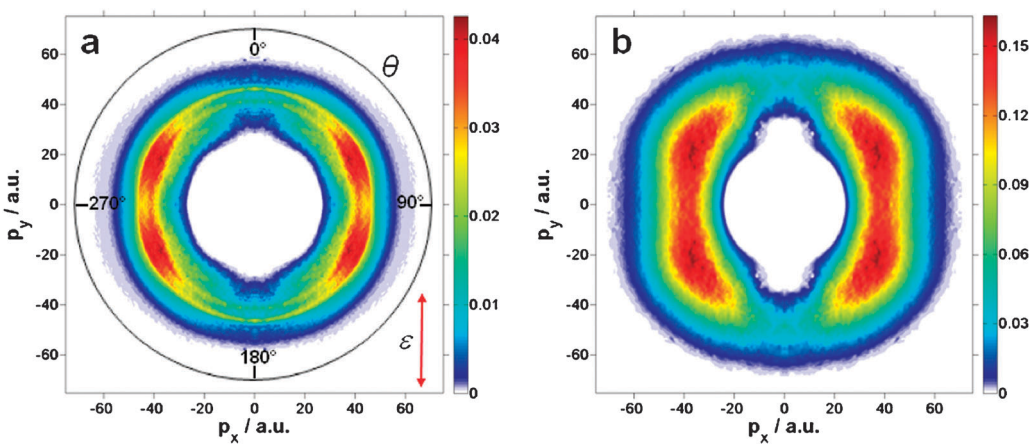

Fig. 1 Momentum distributions (p_y *versus* p_x for p_z = 0) of fragment D^+ (a) and Cl^+ (b) ions from the dissociative ionization of DCl at 1.3×10^{14} W cm^{-2}. The laser is polarized along the y-direction (red arrow). The momentum distributions are averaged over the CEP and left–right as well as up–down symmetrized to increase the signal-to-noise ratio.

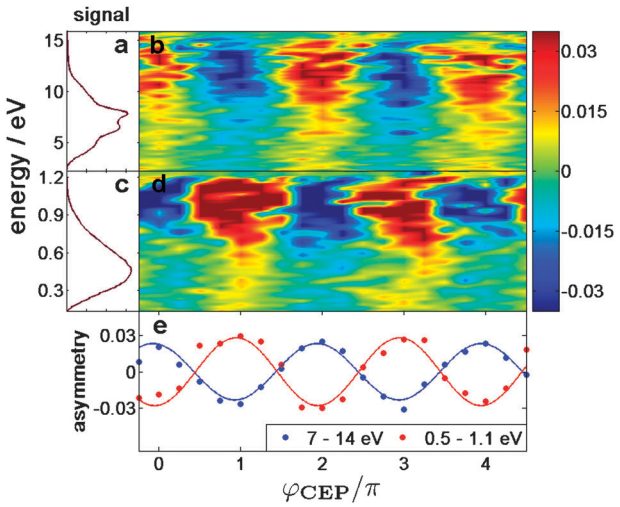

Fig. 2 Fragment ion energy spectra (CEP averaged) and asymmetry maps $A(W, \varphi_{CEP})$ for D^+ ions, (a) and (b), and Cl^+ ions, (c) and (d). $A(W, \varphi_{CEP})$ was obtained by integrating the signal over an angular range from -60° to 60° along the polarization axis. The angular and energy integrated asymmetries $A(\varphi_{CEP})$ for D^+ and Cl^+ ions are shown in (e). Note that $\varphi_{CEP} = \varphi_0 + \varphi$, where the offset phase φ_0 is the same for the data displayed in (b), (d) and (e).

data, the images were left–right symmetrized (with respect to the symmetry axis (p_y)). For each ionic species with mass m and energy $W = p^2/(2m)$ the asymmetry $A(W, \theta, \varphi_{CEP})$ in the ion momentum distribution $P(W, \theta, \varphi_{CEP})$ was obtained for the right half of the image ($p_x > 0$) from

$$A(W,\theta,\varphi_{CEP}) = \frac{P(W,\theta,\varphi_{CEP}) - P(W,\pi-\theta,\varphi_{CEP})}{P(W,\theta,\varphi_{CEP}) + P(W,\pi-\theta,\varphi_{CEP})} \quad \text{for } \theta \in \left[0,\frac{\pi}{2}\right]. \tag{1}$$

The angle integrated asymmetry $A(W, \varphi_{CEP})$ within the angular range [0, α] can then be derived as follows:

$$A(W,\varphi_{CEP}) = \frac{\int_0^\alpha P(W,\theta,\varphi_{CEP})\sin\theta\,d\theta - \int_0^\alpha P(W,\pi-\theta,\varphi_{CEP})\sin\theta\,d\theta}{\int_0^\alpha P(W,\theta,\varphi_{CEP})\sin\theta\,d\theta + \int_0^\alpha P(W,\pi-\theta,\varphi_{CEP})\sin\theta\,d\theta} \tag{2}$$

We chose to analyze the ion emission within a restricted angular range [0, α] with $\alpha = 60^\circ$ to improve the signal-to-noise ratio. These angle integrated asymmetries $A(W, \varphi_{CEP})$ for D^+ and Cl^+ ions from the dissociative ionization of DCl are displayed in Fig. 2b and d. Both asymmetry maps (for D^+ and Cl^+ ions) exhibit an energy independent oscillation with the CEP over the entire range of recorded fragment energies. The two asymmetry maps have been energy integrated to obtain the data points shown in Fig. 2e (the solid lines correspond to fits of the data points to a sine function). The two curves are offset in phase by approximately π.

3. Theoretical results

The ionization of small molecules in strong laser fields has been treated previously with the MO-SFA[28] and MO-ADK[29,30] models. Both approaches provide orientation-dependent ionization rates for ionization from a given molecular orbital (MO), *e.g.* the highest occupied molecular orbital (HOMO), within the one-center approximation. Recent strong-field experiments, however, provided evidence that in molecules with energetically close lying valence orbitals, ionization occurs not only from the HOMO but also from lower lying orbitals, *e.g.* the HOMO − 1.[16,31–33] Moreover, it was shown that for heteronuclear molecules it is important to go beyond the one-center approximation in order to achieve a good agreement with experimental data.[18]

In the heteronuclear molecule DCl the HOMO is a lone-pair 3p Cl-orbital, which is twofold degenerate ($3p_x$, $3p_y$) and thus, ionization from both MOs has to be considered in the theoretical treatment. Here, we use the ansatz of ref. 18 to calculate strong-field ionization probabilities in DCl going beyond the one-center approximation, while taking into account the ionization from the two degenerate HOMOs. A detailed description of the method can be found in ref. 18. In the following we present the most important aspects, necessary to understand the results presented below.

The orientation dependent ionization rate $w(\theta, t)$ of a molecule in an intense laser field can be calculated as the induced electron flux through the barrier of the combined molecular and external electric fields:[34]

$$w(\theta,t) = -\frac{d}{dt}\int_V \rho(\vec{r},\theta,t)\,dV, \tag{3}$$

here $\rho(\vec{r},\theta,t) = \sum_{n\le n_{HOMO}} |\psi_n(\vec{r},\theta,t)|^2$ is the electron density and $\psi_n(\vec{r},\theta,t)$ are the MOs of the molecule in the presence of the external field. The angle θ is the angle between the intramolecular axis and the external field. Within the axial recoil approximation this angle corresponds to the angle θ in the experimental images, under which the fragments formed by the dissociation of the molecule are observed. The MOs are calculated in the adiabatic approximation using a static electric field with the quantum chemistry package Molpro[35] and are represented on a three dimensional grid.

The integral in eqn (4) is taken over the volume V which is confined within a surface S. Following the basic idea of MO-ADK the surface S is spanned by all the outer turning points of $\psi_n(\vec{r},\theta,t_i)$.[34] Beyond these points the exponentially decaying term in the electron wavefunction becomes dominant and the wavefunction enters the classical forbidden region relevant for the tunneling process. The surface S can be determined on the three dimensional grid by numerical evaluation of the first and second derivative of $\psi_n(\vec{r},\theta,t_i)$ starting from maximal $\vec{r}$ values.

In our simulations the ionization probability

$$T(t,\theta;S) = \int_V \rho(\vec{r},\theta,t_i)\,dV - \int_V \rho(\vec{r},\theta,t)\,dV \tag{4}$$

was evaluated numerically at the time t, where the field and hence the ionization rate is maximal. The maximal strength

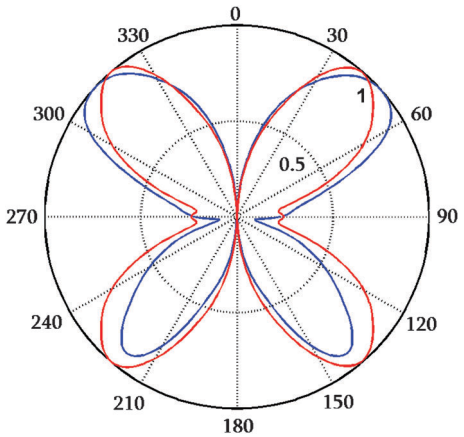

Fig. 3 Calculated angular-dependent relative ionization probability for the HOMOs of DCl at 1.3×10^{14} W cm^{-2}. The symmetric probability (red line) corresponds to a CEP average, while the asymmetric probability (blue line) is obtained for ionization at the field maximum of a cosine-type pulse ($\varphi = 0$).

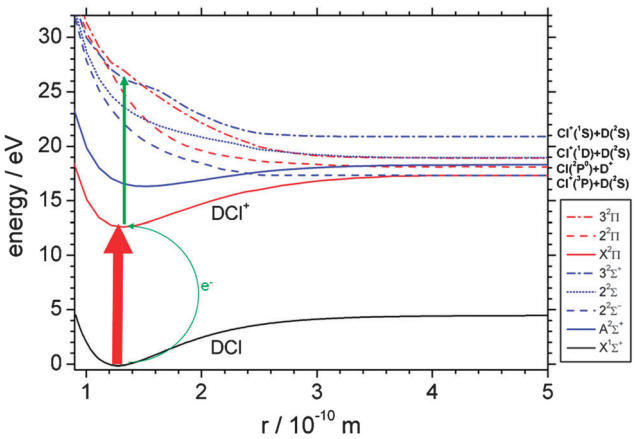

Fig. 4 Relevant potential energy curves for DCl and DCl$^+$ (adapted from ref. 36 and 37). The red arrow indicates tunnel ionization of DCl. The green arrows indicate further excitation by electron recollision with an energy of up to 19.9 eV to excited states of DCl$^+$ including the $2^2\Pi$ state leading to the formation of high energy D$^+$ ions.

and the direction of the field directly depend on the CEP. The initial time t_i corresponds to a time where the electric field is zero. To obtain the orientation dependent ionization probability for a random CEP, we average the ionization probability over the two opposite field directions. Ionization from multiple MOs can also be treated within this ansatz (see ref. 18).

The DCl MO-calculations were performed at the CASSCF(6,9)/6-311G++(2DF,2PD) level of theory and for an electric field strength of 0.06 a.u. (corresponding to the intensity of 1.3×10^{14} W cm^{-2} used in the experiment). In order to account for the random molecular orientations in the experiment, we performed the calculation for 36 orientations θ of the molecule with respect to the laser polarization axis ranging from 0° to 360° in equidistant steps of 10°.

In the hetero-nuclear diatomic DCl the electrons are not symmetrically distributed over the two nuclei, but partially localized on one of the nuclei. Thus one can expect different ionization probabilities for different orientations of the molecule with respect to the external electric field. This effect is averaged out for pulses without phase stabilization, while with phase stabilization it creates an asymmetric angular distribution of the ionized molecules starting from an ensemble of randomly oriented neutral molecules. The calculated asymmetric (blue line; CEP = 0) and symmetric (red line; random CEP) angular dependent ionization probabilities are plotted in Fig. 3. For the asymmetric distribution shown in Fig. 3, the electric field points upwards and DCl is oriented such that the Cl-atom points upwards. Both angular dependent ionization probabilities show distinct maxima around 45°, 135°, 225°, 315° and minima around 0°, 90°, 180° and 270°.

4. Discussion

In order to discuss the angular distribution of fragments in more detail, we show in Fig. 4 the relevant potential energy curves of DCl and DCl$^+$ (adapted from ref. 36 and 37). Tunnel ionization of DCl at a laser intensity of 1.3×10^{14} W cm^{-2} predominantly occurs from the degenerate HOMOs (3p Cl-orbitals)[31] and leads to population of the $X^2\Pi$ electronic ground state of DCl$^+$ (solid red line in Fig. 4). The ejected electron originates from a chlorine lone-pair orbital, which leads to the stable electronic ground state of DCl$^+$, such that neither D$^+$ nor Cl$^+$ ions can be detected after the ionization without additional excitation. The electron that was released upon the ionization of DCl and is accelerated by the oscillatory field of the laser pulse can recollide with the DCl$^+$ ion and lead to further excitation (solid green lines in Fig. 4). At the laser parameters in our experiment, the maximum recollision energy of the electron can be estimated as 3.17 U_p = 19.9 eV. U_p is the ponderomotive potential, defined as $U_p = I/4\omega^2$ (a.u.), where I is the laser intensity. The detection of D$^+$ fragments in the experiment with kinetic energies between 3 and 16 eV (peaking at *ca.* 7.9 eV) indicates that excitation of higher lying states including the $2^2\Pi$ state is important. Dissociation *via* bond softening[38] from either the $X^2\Pi$ or the $A^2\Sigma$ state, which might be reached by a sequential laser excitation by three photons,[31] would lead to low kinetic energies of the D$^+$ and Cl$^+$ fragments. Akagi *et al.* have recently observed fragments from such a dissociation mechanism at kinetic energies below 0.05 eV (Cl$^+$) and below 2 eV (D$^+$).[31] Since the strongest D$^+$ and Cl$^+$ signals are observed at much higher kinetic energies in our experiment, dissociation *via* bond-softening is not considered in the following discussion. After initial population of individual excited states of the DCl$^+$ ion by electron recollision, laser induced coupling of these states might occur. The coupling of various of the repulsive excited states might explain the similar momentum distributions for D$^+$ and Cl$^+$ fragments (since the initial population of a potential leading to D$^+$ fragments could ultimately result in the final formation of Cl$^+$ fragments, similar to what was observed in the case of coupling of excited states of CO$^+$ in a previous experiment).[16] The ring-type pattern observed in the momentum distribution of the D$^+$ fragments shown in Fig. 1 might have a similar origin. Further insight into the fragmentation mechanisms requires advanced

theoretical modeling of the (recollision and) dissociation step, which remains a challenge for future work.

The angular distributions of the D^+ and Cl^+ fragment yields shown in Fig. 1 are similar and peak at around $\pm 60^\circ$ with respect to the laser polarization axis (0°). These angular distributions differ from the orientation dependent ionization probability of the HOMOs (which peaks at $\pm 45^\circ$) and indicate that the angular distribution that is imprinted on the DCl^+ ions in the ionization step is further modified in processes following ionization, *i.e.* recollisional excitation and dissociation.

The angular distribution of the asymmetric D^+ fragment ion emission from the dissociative ionization of DCl at the current laser parameters is further explored in Fig. 5a. The angle dependent asymmetries (see eqn (1)) have been fitted to $A(W, \theta, \varphi_{CEP}) = A_0(W, \theta)\cos(\varphi_{CEP})$ in order to determine the amplitude of the asymmetry $A_0(W, \theta)$ as a function of the kinetic energy W and the fragment emission angle θ. Although CEP-dependent observables do not have to follow a cosine (or sine) function, the fits shown in Fig. 2e give an indication that the asymmetries follow to a good approximation a cosine (or sine)-like behavior. This finding is in agreement with previous studies, where CEP-dependent asymmetries were explored (see *e.g.* ref. 5, 16, 39, and 40). Although the overall asymmetry amplitude is small, it can be seen in Fig. 5a that the absolute value of the asymmetry amplitude $|A_0(W, \theta)|$ peaks at energies in the range between 9 and 14 eV and angles around $\pm 45^\circ$. The amplitude becomes smaller towards emission angles of 0° and $\pm 90^\circ$. In order to show the angular dependence more clearly, the asymmetry map shown in Fig. 5a has been integrated from 6 to 16 eV for the polar presentation shown in Fig. 5b. The butterfly shape of the asymmetry amplitude resembles the orientation dependent ionization probability of the HOMOs (shown as solid line in Fig. 5b). The good agreement between the angular dependence of the asymmetry amplitude and the ionization probability from the HOMOs of DCl suggests that the ionization is responsible for the observed asymmetry in the emission of charged fragments.

The observed π-phase shift in the CEP-dependence of the asymmetry of D^+ and Cl^+ fragments (shown in Fig. 2) further supports the proposed mechanism. Since the DCl^+ ions are partially oriented and their orientation depends on the direction of the electric field, a π phase shift of the electric field also results in a π phase shift of the DCl^+ orientation. The orientation is directly reflected in the asymmetry of the ionic fragment emission.

Although we have not theoretically analyzed any additional contributions to the asymmetry from the dissociation step, preliminary calculations show that these contributions are small at the wavelength used in the current study.[41] This is in contrast to previous theoretical studies at a wavelength around 6.4 μm, where a pronounced CEP dependent asymmetry from the dissociation step was found.[21] A full theoretical treatment of the dissociative ionization of DCl in few-cycle laser fields, including the ionization, recollisional excitation and dissociation steps, is a challenging task for future work.

5. Conclusions

We have studied the dissociative ionization of DCl in phase-stabilized, 5 fs laser fields at 1.3×10^{14} W cm^{-2}. The measured angular distributions of the resulting D^+ and Cl^+ ions are similar and exhibit an anti-correlated CEP dependence. Importantly, the angular distribution of the asymmetry of D^+ ions resembles the orientation-dependent ionization probability of the HOMOs of DCl. These findings indicate that mainly the ionization step is responsible for the asymmetry in the fragment emission. Preferential ionization of DCl molecules with suitable orientation towards the laser electric field permits the control over the orientation of DCl^+ ions, which is reflected in the ionic fragment emission.

We believe that a similar control can be achieved in other heteronuclear molecules with potentially higher degree of orientation. Taking advantage of this control scheme, near single-cycle light fields may be used to produce samples of oriented molecular ions under field-free conditions

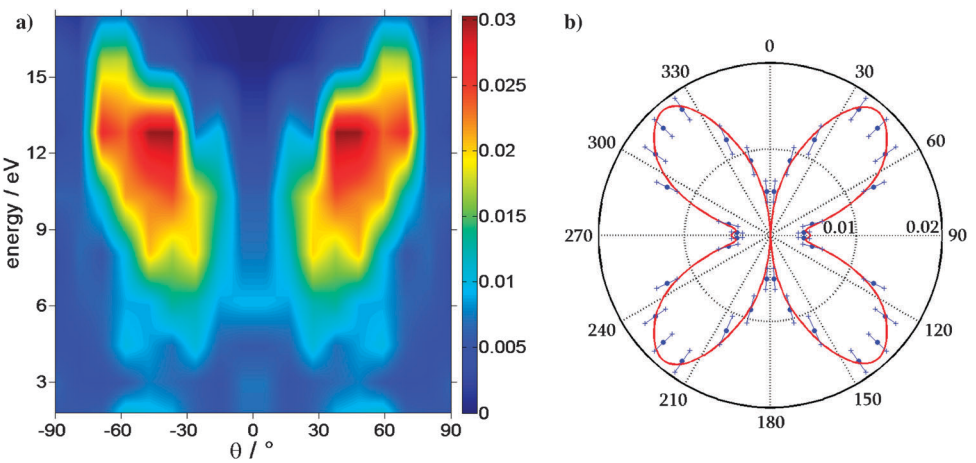

Fig. 5 (a) Absolute value of the asymmetry amplitude $|A_0(W, \theta)|$ of D^+ fragment ions (left–right symmetrized *versus* $\theta = 0$). (b) Polar plot of the energy-integrated (over 6–16 eV) asymmetry derived from (a) (blue dots) as compared to the calculated symmetric ionization probability from the HOMOs of DCl (red line). For visibility, the data and calculated results (which are up–down and left–right symmetric) are shown over a range of 2π.

(which are present after the ionization pulse has passed the sample) suitable for studies on their dynamics in the molecular frame.

Acknowledgements

We acknowledge Marc Vrakking and Ferenc Krausz for their support and the use of specialized equipment. We are grateful for support from the Chemical Sciences, Geosciences, and Biosciences Division, Office of Basic Energy Sciences, Office of Science, U.S. Department of Energy, the National Science Foundation under CHE-0822646 and the DFG *via* the grant We 1330/13, the Emmy-Noether program, the International Collaboration in Chemistry program and the Cluster of Excellence: Munich Center for Advanced Photonics (MAP).

References

1 R. Kienberger, M. Uiberacker, M. F. Kling and F. Krausz, *J. Mod. Opt*., 2007, **54**, 1985.
2 K. M. Weitzel, *ChemPhysChem*, 2007, **8**, 213.
3 M. F. Kling, C. Siedschlag, A. J. Verhoef, J. I. Khan, M. Schultze, T. Uphues, Y. Ni, M. Uiberacker, M. Drescher, F. Krausz and M. J. J. Vrakking, *Science*, 2006, **312**, 246.
4 M. F. Kling, C. Siedschlag, I. Znakovskaya, A. J. Verhoef, S. Zherebtsov, F. Krausz, M. Lezius and M. J. J. Vrakking, *Mol. Phys*., 2008, **106**, 455.
5 M. Kremer, B. Fischer, B. Feuerstein, V. L. B. de Jesus, V. Sharma, C. Hofrichter, A. Rudenko, U. Thumm, C. D. Schröter, R. Moshammer and J. Ullrich, *Phys. Rev. Lett*., 2009, **103**, 213003.
6 A. D. Bandrauk, S. Chelkowski and H. S. Nguyen, *Int. J. Quantum Chem*., 2004, **100**, 834.
7 D. Geppert, P. von den Hoff and R. de Vivie-Riedle, *J. Phys. B: At., Mol. Opt. Phys*., 2008, **41**, 074006.
8 S. Gräfe and M. Y. Ivanov, *Phys. Rev. Lett*., 2007, **99**, 163603.
9 V. Roudnev, B. D. Esry and I. Ben-Itzhak, *Phys. Rev. Lett*., 2004, **93**, 163601.
10 X. M. Tong and C. D. Lin, *Phys. Rev. Lett*., 2007, **98**, 123002.
11 P. Brumer and M. Shapiro, *Chem. Phys. Lett*., 1986, **126**, 541.
12 M. Shapiro, J. W. Hepburn and P. Brumer, *Chem. Phys. Lett*., 1988, **149**, 451.
13 R. J. Gordon and S. A. Rice, *Annu. Rev. Phys. Chem*., 1997, **48**, 601.
14 S.-P. Lu, S. M. Park, Y. Xie and R. J. Gordon, *J. Chem. Phys*., 1992, **96**, 6613.
15 D. Ray, F. He, S. De, W. Cao, H. Mashiko, P. Ranitovic, K. P. Singh, I. Znakovskaya, U. Thumm, G. G. Paulus, M. F. Kling, I. V. Litvinyuk and C. L. Cocke, *Phys. Rev. Lett*., 2009, **103**, 223201.
16 I. Znakovskaya, P. von den Hoff, S. Zherebtsov, A. Wirth, O. Herrwerth, M. J. J. Vrakking, R. de Vivie-Riedle and M. F. Kling, *Phys. Rev. Lett*., 2009, **103**, 103002.
17 P. von den Hoff, I. Znakovskaya, M. F. Kling and R. de Vivie-Riedle, *Chem. Phys*., 2009, **366**, 139.
18 P. von den Hoff, I. Znakovskaya, S. Zherebtsov, M. F. Kling and R. de Vivie-Riedle, *Appl. Phys. B: Lasers Opt*., 2010, **98**, 659.
19 H. G. Breunig, A. Lauer and K. M. Weitzel, *J. Phys. Chem. A*, 2006, **110**, 6395.
20 M. V. Korolkov and K. M. Weitzel, *J. Chem. Theory Comput*., 2006, **2**, 1492.
21 M. V. Korolkov and K. M. Weitzel, *Chem. Phys*., 2007, **338**, 277.
22 A. J. Verhoef, A. Fernandez, M. Lezius, K. O'Keeffe, M. Uiberacker and F. Krausz, *Opt. Lett*., 2006, **31**, 3520.
23 S. Micheau, Z. Chen, A. T. Le, J. Rauschenberger, M. F. Kling and C. D. Lin, *Phys. Rev. Lett*., 2009, **102**, 073001.
24 A. T. J. B. Eppink and D. H. Parker, *Rev. Sci. Instrum*., 1997, **68**, 3477.
25 O. Ghafur, W. Siu, P. Johnsson, M. F. Kling, M. Drescher and M. J. J. Vrakking, *Rev. Sci. Instrum*., 2009, **80**, 033110.
26 M. F. Kling, J. Rauschenberger, A. J. Verhoef, E. Hasovic, T. Uphues, D. B. Milosevic, H. G. Muller and M. J. J. Vrakking, *New J. Phys*., 2008, **10**, 025024.
27 M. J. J. Vrakking, *Rev. Sci. Instrum*., 2001, **72**, 4084.
28 J. Muth-Böhm, A. Becker and F. H. M. Faisal, *Phys. Rev. Lett*., 2000, **85**, 2280.
29 X. M. Tong, Z. Zhao and C. D. Lin, *Phys. Rev. A: At., Mol., Opt. Phys*., 2002, **66**, 033402.
30 S. F. Zhao, C. Jin, A. T. Le and C. D. Lin, *Phys. Rev. A: At., Mol., Opt. Phys*., 2010, **82**, 035402.
31 H. Akagi, T. Otobe, A. Staudte, A. Shiner, F. Turner, R. Dörner, D. M. Villeneuve and P. B. Corkum, *Science*, 2009, **325**, 1364.
32 B. K. McFarland, J. P. Farrell, P. H. Bucksbaum and M. Gühr, *Science*, 2008, **322**, 1232.
33 O. Smirnova, Y. Mairesse, S. Patchkovskii, N. Dudovich, D. Villeneuve, P. Corkum and M. Y. Ivanov, *Nature*, 2009, **460**, 972.
34 B. M. Smirnov and M. I. Chibisov, *JETP Lett. Engl. Transl*., 1966, **22**, 585.
35 H. J. Werner and P. J. Knowles *et al*., *Molpro*, *version 2006.1*, 2006.
36 V. S. Gurin, M. V. Korolkov, V. E. Matulis and S. K. Rkhmanov, *J. Chem. Phys*., 2007, **126**, 124321.
37 A. D. Pradhan, K. P. Kirby and A. Dalgarno, *J. Chem. Phys*., 1991, **95**, 9009.
38 P. H. Bucksbaum, A. Zavriyev, H. G. Muller and D. W. Schumacher, *Phys. Rev. Lett*., 1990, **64**, 1883.
39 N. G. Johnson, O. Herrwerth, A. Wirth, S. De, I. Ben-Itzhak, M. Lezius, B. Bergues, M. F. Kling, A. Senftleben, C. D. Schröter, R. Moshammer, J. Ullrich, K. J. Betsch, R. R. Jones, A. M. Sayler, T. Rathje, K. Rühle, W. Müller and G. G. Paulus, *Phys. Rev. A: At., Mol., Opt. Phys*., 2011, **83**, 013412.
40 M. F. Kling and M. J. J. Vrakking, *Annu. Rev. Phys. Chem*., 2008, **59**, 463.
41 M. V. Korolkov and K. M. Weitzel, unpublished.

